THE ASTROPHYSICAL JOURNAL, 380:140–150, 1991 October 10

H II REGION ABUNDANCES: MODEL OXYGEN LINE RATIOS

STACY S. MCGAUGH
Department of Astronomy, University of Michigan, Ann Arbor, MI 48109
Received 1991 January 31; accepted 1991 April 24

ABSTRACT

We present an extensive, homogeneous grid of H II region models. We find that the behavior of the strong oxygen lines can be modeled by taking proper account of the softening of the ionizing spectra produced by stars of increasing metallicity. This provides a calibration of the abundance indicating line ratio ([O II] λ3727 + [O III] $\lambda\lambda$4959, 5007)/Hβ which is comparable in accuracy to that obtainable by direct methods when a temperature-sensitive line ratio is available.

No metallicity dependence of the IMF is required to explain the systematic softening of stellar spectra with increasing metallicity. It results naturally from the stellar mass-temperature-metallicity relation. Also, we find no convincing evidence for a correlation between the ionization parameter and metallicity which cannot be attributed to observational selection effects. Hence it remains possible that the extragalactic H II region excitation sequence is purely a metallicity effect.

Subject headings: nebulae: abundances — nebulae: H II regions

1. INTRODUCTION

The emission-line spectra of giant H II regions—those ionized by large clusters of OB stars—provide a powerful probe of conditions in other galaxies. In particular, gas phase abundances of many elements can be derived with accurate measurement of temperature-sensitive line ratios, such as [O III] $\lambda\lambda$4959, 5007/λ4363 (Osterbrock 1989). Unfortunately, λ4363 and its analogs are too weak to be measured in most extragalactic objects. However, the intensities of the most prominent oxygen lines are correlated with metallicity due to the shifting of the cooling from the optical forbidden lines to the infrared "fine-structure" lines as the electron temperature drops with the increasing abundance of coolants. Hence it is possible to construct "empirical" abundance indicators which make use of the more readily observable lines. Such methods were proposed by Alloin et al. (1979) and Pagel et al. (1979). The latter, $R_{23} \equiv$ ([O II] λ3727 + [O III] $\lambda\lambda$4959, 5007)/Hβ, has found widespread acceptance and use.

Accordingly, substantial effort has been put into calibrating R_{23}: Pagel et al. (1979), Pagel, Edmunds, & Smith (1980), Edmunds & Pagel (1984, hereafter EP), McCall, Rybski, & Shields (1985, hereafter MRS), Dopita & Evans (1986, hereafter DE), Torres-Peimbert, Peimbert, & Fierro (1989, hereafter TPF), and Skillman (1989, hereafter S89). Obtaining the correct calibration has been difficult, because the calibrating data points require an oxygen abundance determined with an independent measure of electron temperature (i.e., λ4363). This information is typically only available in the regime where the oxygen lines are strongest, $Z < 0.5\ Z_\odot$. At higher abundances, one must use a different method, such as detailed model fits to the data. Also, the paucity of data with good independent measures of the electron temperature has led to the use of all available data in the calibration; however, the various data sets were selected in different ways: some by galaxy (e.g., the bright H II regions of M101), some by objective prism (which are biased towards strong [O III] $\lambda\lambda$4959, 5007), some by type (dwarf irregulars). The heterogeneity in both method and data cause some concern about the reliability of the calibration. This is reflected in the variety of differing calibrations in the literature (see Fig. 1).

This motivates a systematic investigation which is uniform in method. Since the data currently available are not sufficient for this, we take a theoretical approach. For R_{23} to work as an abundance sequence, the volume of parameter space occupied by real H II regions must be a systematic function of metallicity (see below). Based on the observation that the equivalent width of Hβ decreases with increasing abundance (Searle 1971), Pagel et al. (1979) realized that this systematic variation must be due to an anticorrelation between stellar temperature and oxygen abundance. Indeed, this behavior is expected from basic stellar physics, and forms the basis of our approach.

2. MODELS

The H II region models are specified by three parameters: the shape of the ionizing spectrum (T), the geometry of the nebula ($\bar{U}$), and the abundance of the chemical elements in the gas (Z). Our grid covers a wide range of these parameters, described in detail below. The photoionization code CLOUDY (Ferland & Truran 1981) was used to compute the nebular spectra based on these inputs. We also consider the effect of dust within the nebula by comparing two otherwise identical grids, one containing dust and the other not. The two grids comprise a total of 168 individual models.

2.1. *Ionizing Spectra*

The ionizing spectra are produced by clusters of OB stars. The spectra are calculated by convolving the model atmospheres of Mihalas (1972) with a stellar mass spectrum (the initial mass function, or IMF). A unique spectrum is calculated for each IMF *and* metallicity. That is, the effective temperatures of the stars are assumed to be a function $T(M, Z)$ of both mass and metallicity. This is achieved by interpolating through the model grid of Maeder (1990), which gives stellar evolutionary tracks for a number of masses *and* metallicities. Prior to these models, adequate information on massive stars of nonsolar metallicity was not available. Hence, previous workers were restricted to assuming that stellar effective temperature was a function of mass only, and they could at best make corrections for the depths of metal edges at various metallicities (Shields & Searle 1978). This method may give an

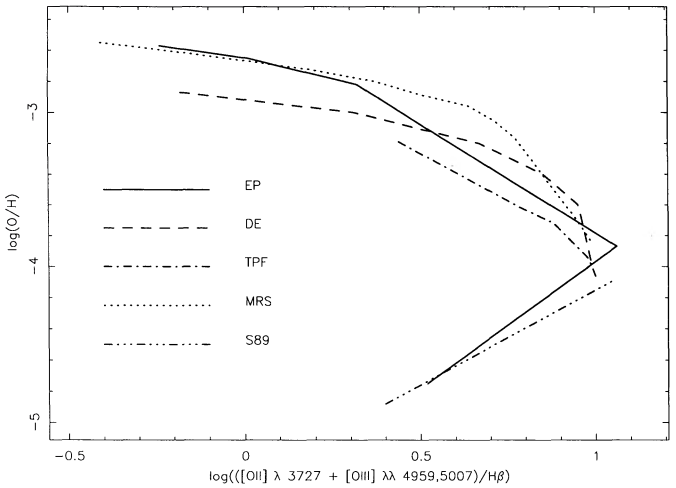

FIG. 1.—Published calibrations of the abundance indicator R_{23}. *Solid line*: Edmunds & Pagel (1984). *Dashed line*: Dopita & Evans (1986). *Dash-dotted line*: Torres-Peimbert, Peimbert, & Fierro (1989). *Dotted line*: McCall, Rybski, & Shields (1985). *Dash-triple dotted line*: Skillman (1989).

accurate representation of the variation of the stellar spectra at a particular effective temperature, but it cannot account for the difference in temperature of stars of the same mass but different metallicity. This can be severe: in the models of Maeder (1990), a 60 $M_\odot$ star with $Z = 0.1\ Z_\odot$ has the same effective temperature as a 120 $M_\odot$ star with $Z = 2\ Z_\odot$ (see Fig. 2).

Armed with the full $T(M, Z)$ relation provided by Maeder (1990), we proceed to construct the ionizing spectra produced by star clusters of metallicity equal to that of the gas in the nebula. We assume that the IMF is fixed and is in no way a function of Z. For an IMF

$$\Psi(M) = AM^{-\Gamma}\ , \tag{1}$$

where A is a normalization constant and Γ is the slope, the flux of the stellar population is

$$F(\lambda) = \int_{M_l}^{M_u} \Psi(M) F(\lambda, M) dM\ , \tag{2}$$

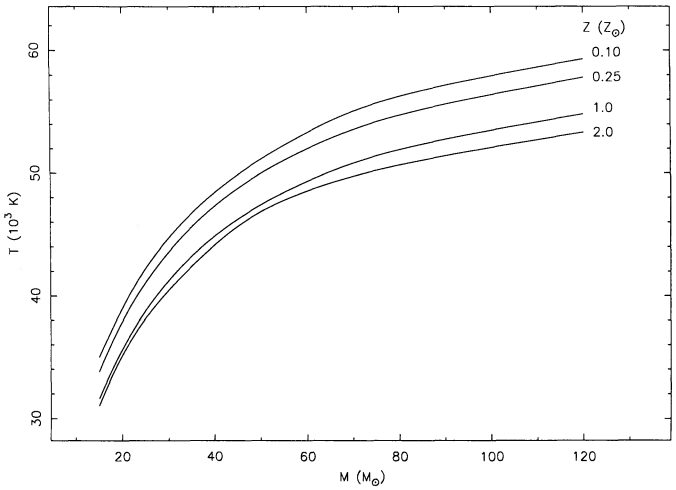

FIG. 2.—Mass-temperature-metallicity [$T(M, Z)$] relation from the models of Maeder (1990). Stellar temperature is given as a function of mass with loci of different metallicity labeled.

which is approximated by

$$F(\lambda) \approx \sum_{M_l}^{M_u} \Psi_M F_M(\lambda)\ . \tag{3}$$

The flux must be approximated in this way because we are employing a finite grid of model atmospheres to represent the flux contributed by each star of mass M. It is thus necessary to interpolate and occasionally extrapolate the $T(M, Z)$ relation to find the mass of the star with an effective temperature for which we have a model atmosphere at each metallicity. This mass is then used to compute the relative number of stars Ψ_M with that known spectrum. This essentially weights the contribution of each atmosphere represented in the grid by the number of stars of that temperature. The model atmosphere flux must also be weighted by the surface area of each star; this is obtained from $L \propto R^2$ with the assumption of constant $\log(g)$ as is appropriate for the atmospheres used.

These are the $\log(g) = 4$, NLTE atmospheres of Mihalas (1972). They go up to $T = 55{,}000$ K in steps of 5000 and are plotted in Figure 3. Stars with $T < 35{,}000$ K do not contribute significantly to the ionizing flux and can be ignored. The choice of atmospheres is somewhat arbitrary. In principle one wants a set of atmospheres which includes all the relevant effects: differing line blanketing with metallicity, various surface gravities, NLTE, etc. (see discussion in S89). In practice such models do not exist. Since blanketed models matched to the metallicities of the nebular gas are not available, the unblanketed NLTE models were selected. Line blanketing effects are less severe in NLTE models than in LTE ones, and NLTE effects are important in hot stars. Hence these atmospheres are reasonable approximations to the spectra of stars at all metallicities. Indeed, Evans (1991) finds that adjusting the metallicity of these atmospheres with the method of Shields & Searle (1978) has virtually no effect on the resultant nebular spectrum.

The choice of IMF is also fraught with uncertainty. The slope Γ is uncertain for massive stars; fortunately, the shape of the ionizing spectrum is insensitive to this (see Fig. 4). Massey, Parker, & Garmany (1989) find $\Gamma \approx 1.9$; we adopt $\Gamma = 2$ as a working value. Since low-mass stars produce insignificant numbers of ionizing photons, these calculations are insensitive to M_l. There is considerable sensitivity to M_u, so we investigate several values of this parameter: $M_u = 100\ M_\odot$, $60\ M_\odot$, and 25

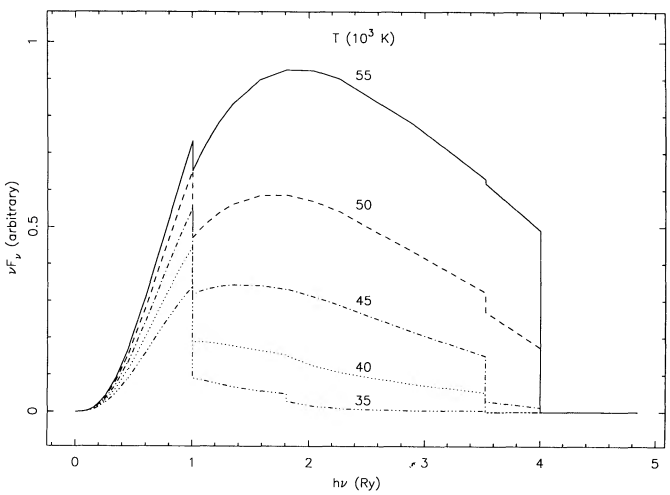

FIG. 3.—NLTE stellar atmospheres of Mihalas (1972)

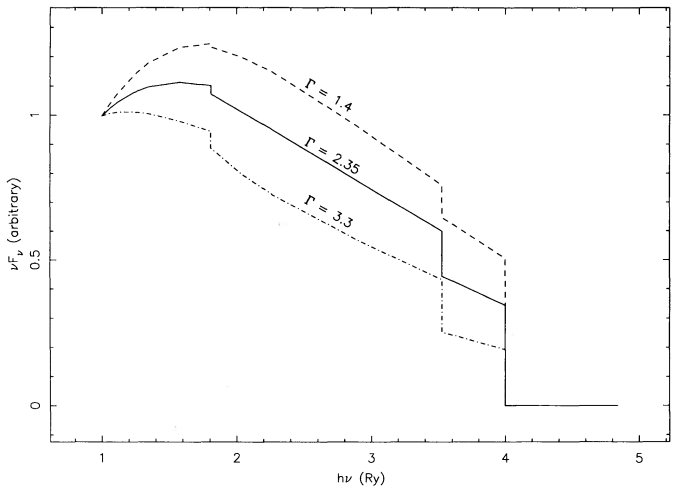

FIG. 4.—Ionizing spectra produced by clusters with different IMF slopes Γ. The *shape* of the spectra is not very sensitive to Γ.

$M_\odot$. The choice of these values is made so as to minimize the effects of the discontinuous approximation to the IMF made in equation (3). While it is unlikely that M_u is as low as 25 $M_\odot$, one can also think of these models as representing evolved clusters with main sequence turnoff masses equal to M_u.

The resulting spectra are presented in Figure 5. For each M_u, the spectra for all the metallicities in the grid are plotted. The crucial point to note is that *the spectra soften significantly as Z increases.* This theoretical result is in agreement with the observational result of Vilchez & Pagel (1988). However, it is obtained naturally from the $T(M, Z)$ relation, and does not imply a metallicity-dependent IMF as Vilchez & Pagel (1988) suppose.

Physically, this softening is what drives R_{23} as an abundance indicator, and is why our models are unique from previous efforts. Note also that the total ionizing luminosity does not change much with metallicity (see Fig. 5). This is because the stars grow more luminous with increasing Z as well as becoming cooler; these effects tend to cancel one another resulting in relatively constant ionizing luminosity. There does seem to be a tendency for the Lyman continuum luminosity to decline more rapidly at high metallicity than at low metallicity as the cluster evolves (e.g., as M_u declines), an effect which would be enhanced if metal-rich stars evolve more rapidly than metal-poor stars. For some typical distribution of ages, this would result in fewer luminous H II regions in metal-rich regions; this effect is in itself too small to explain the large differences in the H II region luminosity function seen in different Hubble types (Kennicutt, Edgar, & Hodge 1989), but may be a contributing factor.

At a given M_u, the sudden jump in Figure 5 between $Z = 0.3$ $Z_\odot$ and 0.75 $Z_\odot$ is due to the loss of the hottest atmosphere represented in the IMF between these metallicities (i.e., the discontinuous IMF approximation previously mentioned). While a more continuous set of atmospheres is desirable, what is important is *some* implementation of the $T(M, Z)$ relation. Indeed, the construction of cluster spectra is a step forward; most work in this field has represented the cluster spectra with a single stellar atmosphere. This "δ-function" approximation to the IMF misses important differences in the shapes of the spectra (compare Figs. 3 and 5). In particular, the IMF spectra have relatively more soft photons and different absorption edge depths.

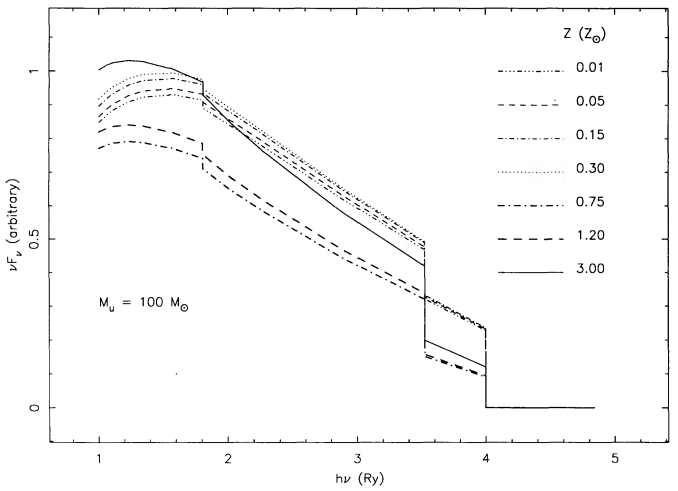

FIG. 5a

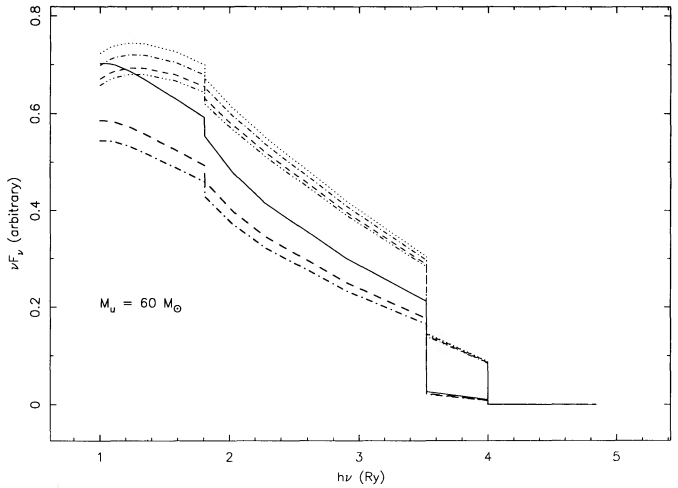

FIG. 5b

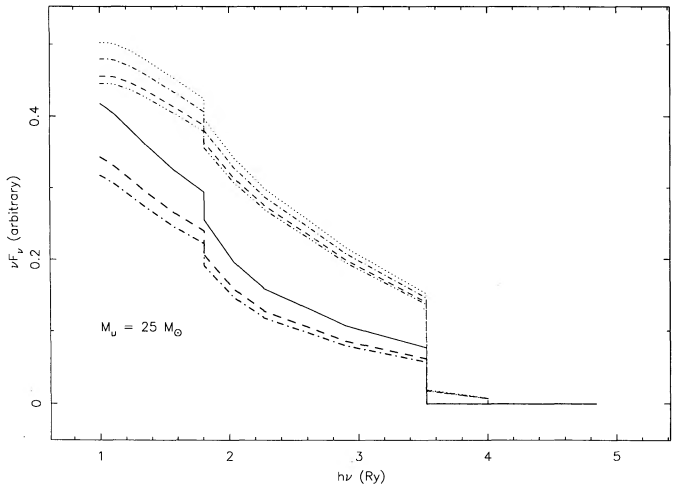

FIG. 5c

FIG. 5.—Ionizing spectra employed in the H II region model grid for various IMF upper mass cutoffs, which can also be viewed as main-sequence turnoff masses. (*a*) $M_u = 100$ $M_\odot$, (*b*) $M_u = 60$ $M_\odot$, (*c*) $M_u = 25$ $M_\odot$. Lines corresponding to the seven metallicities represented in the grid are labeled in (*a*) Note that while the units of the ordinate are arbitrary, the scale is the same for all three graphs so that the fluxes produced at each M_u are directly comparable. Also note that the variation in flux between different metallicities at the same M_u is the result of the discontinuous approximation to the IMF induced by the finite grid of model atmospheres (see text).

Finally, it is important to realize that the stellar population which produces the ionizing continuum is very complicated. The massive stars with which we are concerned evolve on very short time scales which are comparable to the duration of star-formation events. This means that there is no simple, single generation of massive stars; differences in the time of birth are evident in cluster HR diagrams (Massey et al. 1989). In constructing our cluster spectra, we have assumed that all stars are on the zero-age main sequence. This is probably not the case, and since Maeder's (1990) models include evolutionary information, a more sophisticated approach is possible. However, simplifying assumptions must still be made about the distribution of birth times, and atmospheres appropriate to the evolved stars are not readily available. Since the main sequence is the longest phase of the stars' lives, and most of the ionizing photons are produced by the main sequence (von Hippel & Bothun 1990), the treatment of the spectra of evolved clusters as being produced only by stars still on the main sequence (e.g., $M \leq M_u$) seems quite adequate given the uncertainty in the actual distribution of stars in the HR diagram (which is probably unique to each cluster) and the uncertainty of the actual spectra produced by the stars. It will be shown that *at a particular metallicity and geometry*, the oxygen lines are not particularly sensitive to M_u and the shape of the ionizing spectrum.

2.2. *Nebular Geometry*

The geometry of our model nebulae is a constant density (100 cm^{-3}), spherical gas with nonunity filling factor ϵ. The ionizing cluster is treated as a point source at the center of the gas cloud. The photoionization calculation is stopped when the electron density falls to 1% of the hydrogen density. We delineate differing geometries by varying the filling factor and label the models by their volume averaged ionization parameter $\bar{U}$. The ionization parameter is the ratio of ionizing photon density to gas density and is a strong function of position within the nebula:

$$U(R) = \frac{Q}{4\pi c N R^2}, \tag{4}$$

where Q is the ionizing luminosity (set to a typical value of $\log Q = 52.23$ photons s^{-1}), N is the gas density, and R is the distance from the ionizing source. The volume averaged ionization parameter $\bar{U}$ is

$$\bar{U} = \frac{\int_0^{R_s} U(R) dV}{\int_0^{R_s} dV}, \tag{5}$$

with $dV = 4\pi R^2 dR$ and the Strömgren radius $R_s = (3Q/4\pi\epsilon\alpha N^2)^{1/3}$, α being the case B hydrogen recombination coefficient. For constant density models, $\bar{U}$ is simply

$$\bar{U} = \frac{3Q}{4\pi c N R_s^2}. \tag{6}$$

We take this to be characteristic of the geometry of the nebula. Our grid includes values of $\bar{U} = 0.0001$, 0.001, 0.01, and 0.1, which is quite sufficient to cover the volume of parameter space occupied by observed H II regions (intermediate values are typical).

Note that while ϵ is the functional variable with N and Q fixed (models with different N and Q but identical $\bar{U}$ are approximately homologous), α is a function of electron temperature. Since the temperature of the model is not known a priori, R_s does vary from the expected value, which is evaluated at $T_e = 10^4$ K. The effect is weak, since $R_s \propto \alpha^{-1/3}$, and $\alpha \propto T_e^{-1}$. The effect of dust on R_s is more severe (see § 2.4). Also, density variations can have nonhomologous effects at low excitation as a result of the importance of infrared lines with low critical densities (Stasinska 1990; Oey & Kennicutt 1991). Thus the actual ionization parameter is slightly different than the label $\bar{U}$. Nevertheless, we feel that $\bar{U}$ is a good characteristic since it fairly describes how the models were set up to have identical geometry (ϵ, N, Q) at a given $\bar{U}$.

2.3. *Chemical Abundances*

The model grid consists of seven metallicities ranging from $Z = 0.01\ Z_\odot$ to $3\ Z_\odot$. Since oxygen is the main coolant in the model nebulae and is the primary contributor to baryonic mass among metals, its ratio to hydrogen is treated as the variable Z, and all other metal abundances are referenced to it. The abundance of the elements relative to oxygen vary from their solar ratios at different Z.

Different stellar mass ranges contribute different elements to the nucleosynthetic history of the observable gas in a galaxy. Since the different mass ranges return their nucleosynthesis products to the gas on different time scales and in different ways, one expects the exact composition of any particular region to depend on time, place, and star-formation history. Accordingly, one does not expect the relative abundances of the heavy elements to remain fixed. Recent data indicate that this is in fact the case, and can be used to construct an abundance grid which better approximates reality than the simple assumption of variation in lockstep. The treatment the elements included in our models is detailed below.

2.3.1. *Helium*

Most of the helium in the universe is primordial. However, some fraction must be due to stellar production. This can be expressed as

$$Y = Y_p + \frac{\partial Y}{\partial Z} Z, \tag{7}$$

where Y_p is the primordial mass fraction and $\partial Y/\partial Z$ is the rate of helium production. While Y_p may be accurately known, $\partial Y/\partial Z$ is not (Pagel, Terlevich, & Melnick 1986). By number, we take

$$\mathrm{He/H} = 0.0772 + 15(\mathrm{O/H}), \tag{8}$$

where we have chosen $\partial Y/\partial Z$ to reproduce the solar helium abundance at solar metallicity.

2.3.2. *Nitrogen*

The nucleosynthetic status of nitrogen is unclear. It has been suggested that nitrogen should be a secondary element with N/O $\propto$ O/H (Talbot & Arnett 1975), but some data suggest the existence of a primary component (Pagel & Edmunds 1981; Dufour, Garnett, & Shields 1988). We take

$$\log(\mathrm{N/O}) = 0.5 \log(\mathrm{O/H}) + 0.4, \tag{9}$$

in accordance with the observations of TPF. This intermediate value for the slope may be the result of the data sampling a transition region between primary and secondary modes of production. If so, equation (9) will slightly underestimate the nitrogen abundance at both extremely high and extremely low Z.

2.3.3. *Iron*

The iron abundance does not vary in lockstep with oxygen. Since [Fe/H] is what is traditionally quoted for the metallicities of stars, and [O/H] is what is determined for H II regions, there has been considerable difficulty in comparing the two. The variation is in the sense that when [Fe/H] has dropped to very low values, [O/H] is still reasonably large. This means that the mass in heavy elements is not as low as is implied by [Fe/H] as [O/H] ≈ -1 when [Fe/H] ≈ -2. The data of Abia & Rebolo (1989), which shows a slight change in behavior at $\log(\mathrm{O/H}) \approx -4$, were used to determine the approximate relations

$$\log(\mathrm{FeO}) = 1.17 \log(\mathrm{O/H}) + 1.70 \quad \text{for } \log(\mathrm{O/H}) > -4\,, \tag{10a}$$

$$\log(\mathrm{Fe/O}) = 0.35 \log(\mathrm{O/H}) - 1.58 \quad \text{for } \log(\mathrm{O/H}) < -4\,. \tag{10b}$$

2.3.4. *Carbon*

Carbon roughly tracks iron down to $\log(\mathrm{O/H}) \approx -4$, then it too changes behavior. The data of Tomkin, Sneden, & Lambert (1986) were used to determine the relations

$$\log(\mathrm{C/O}) = 1.17 \log(\mathrm{O/H}) + 3.23 \quad \text{for } \log(\mathrm{O/H}) > -4\,, \tag{11a}$$

$$\log(\mathrm{C/O}) = -0.70 \log(\mathrm{O/H}) - 4.26 \quad \text{for } \log(\mathrm{O/H}) < -4\,. \tag{11b}$$

Note that because the slope in equation (11a) is greater than 1, carbon will become more numerous than oxygen at $\log(\mathrm{O/H}) = -2.76$ if this trend continues. Indeed, these data hint that carbon is produced slightly *more* rapidly than iron, so that the slope of equation (11a) should be even steeper. A steeper slope would reproduce the solar C/O ratio better than equation (11a), but the data are too uncertain to yield a better value.

2.3.5. *Other Elements*

Also included are neon, magnesium, aluminum, silicon, sulfur, argon, and calcium. These are assumed to remain fixed in abundance relative to oxygen. Most are α-process elements and should behave in this fashion. For neon, argon, and sulfur, this is consistent with the observations of TPF. The adopted ratios are Ne/O = 0.20, Mg/O = 0.05, Al/O = 0.004, Si/O = 0.052, S/O = 0.025, Ar/O = 0.007, Ca/O = 0.0028.

The abundance grid derived from these relations is reproduced in Table 1. While these values are rather uncertain, they fairly represent the observed trends in elemental abundance ratios. Since oxygen is the primary H II region coolant, minor variations from this grid will not affect our results.

2.4. *Dust*

Real H II regions are observed to contain considerable amounts of dust. This is no doubt important to the physics of the nebulae; unfortunately, we know far too little about the dust to model its effects in detail. Nonetheless, CLOUDY has the ability to include dust as described by Martin & Ferland (1980). To gauge the importance of dust, we computed two complete model grids, differing only in the inclusion or exclusion of dust. In the dusty models, it was assumed that the dust to gas ratio increases as a linear function of Z, reaching the solar neighborhood value at solar metallicity.

TABLE 1

ABUNDANCE GRID

Z	He	C	N	O	Fe
0.01.....	−1.11	−5.79	−7.25	−5.10	−8.47
0.05.....	−1.11	−5.58	−6.20	−4.40	−7.52
0.15.....	−1.10	−5.23	−5.45	−3.90	−6.76
0.30.....	−1.09	−4.58	−5.00	−3.60	−6.11
0.75.....	−1.07	−3.71	−4.40	−3.20	−5.24
1.20.....	−1.04	−3.28	−4.10	−3.00	−4.81
3.00.....	−0.96	−2.41	−3.50	−2.60	−3.94

NOTES.—All entries are logarithmic abundances by number relative to hydrogen, except for Z which is linear in terms of $Z_\odot$. For clarity, those elements whose abundance is fixed relative to oxygen are omitted.

The primary effect of dust is to compete with hydrogen for *absorption* of ionizing photons. This results in a decrease in the Balmer line luminosity of the nebula and a shrinkage of the Strömgren sphere. The loss of optical luminosity can be severe (see Fig. 6) and is probably the cause of the low Hβ equivalent widths observed at high metallicity (Searle 1971). This may help to explain why very large, luminous extragalactic H II regions are preferentially seen in low-metallicity environments (Kennicutt et al. 1989), and is important to the determination of star formation rates based on Hα luminosities, where *scattering* opacity due to dust is already the greatest uncertainty (Kennicutt 1983).

For our current purposes, the shrinkage of the Strömgren sphere makes the dusty H II region models look like dust-free models of slightly higher $\bar{U}$. Real dust no doubt has other effects as well; for example, certain elements should be depleted onto the dust. However, this would just reduce the gas phase abundance of these coolants, making oxygen even more dominant in this role. Since dust-free models provide good fits to real H II regions, and the dusty models are qualitatively similar, it seems unlikely that any missing effects of the dust would alter things seriously.

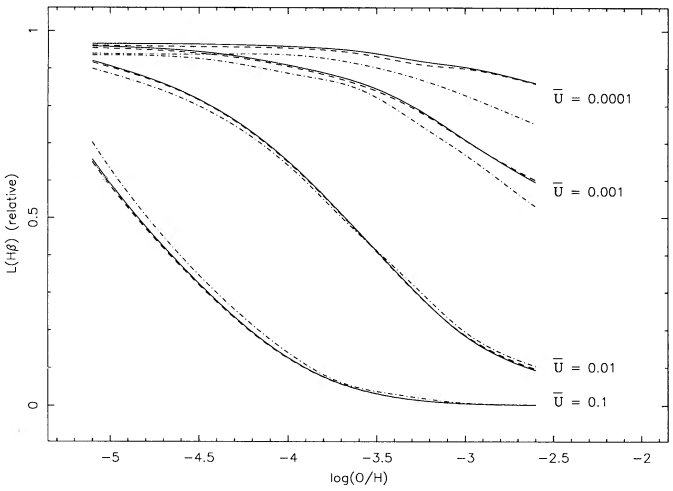

FIG. 6.—Hβ luminosity of dusty models relative to that expected from the assumption that every Lyman continuum photon ionizes one hydrogen atom. This ratio is never unity since some photons are absorbed by helium; at high metallicity absorption by dust is significant (assuming the dust to gas ratio increases linearly with metallicity and that the two are uniformly mixed). The models fall into families by geometry (labeled with the ionization parameter $\bar{U}$). Different M_u are represented by different lines. *Solid line*: $M_u = 100\ M_\odot$. *Dashed line*: $M_u = 60\ M_\odot$. *Dash-dotted line*: $M_u = 25\ M_\odot$.

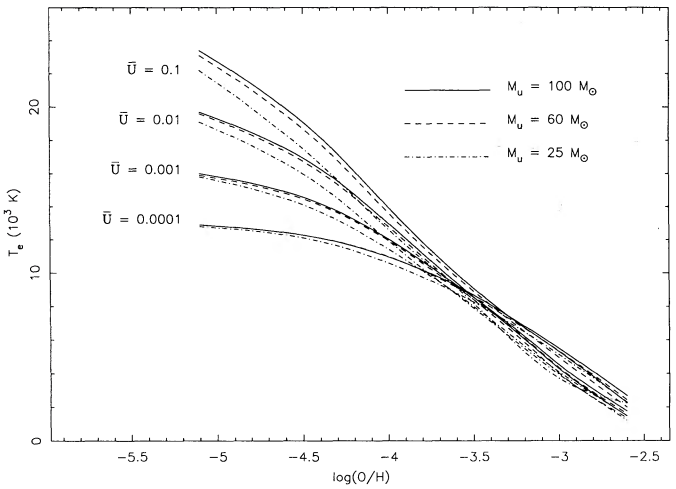

FIG. 7.—Average electron temperatures of the models as a function of metallicity. Again, the models fall into families labeled by $\bar{U}$, and the different M_u are represented by different lines, as per Fig. 6.

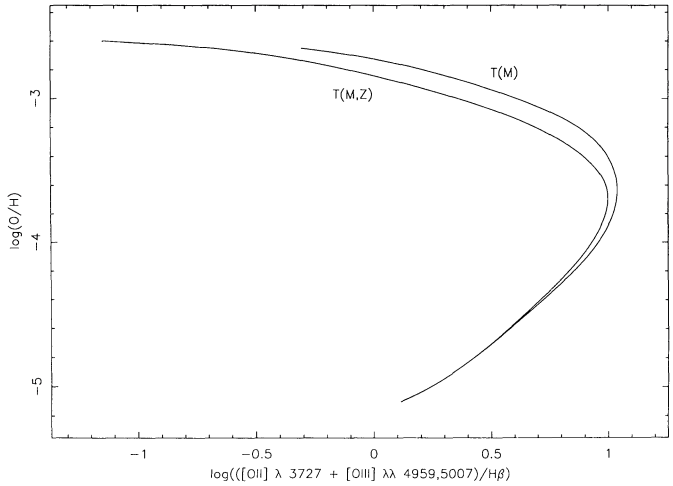

FIG. 8.—Comparison of the behavior of R_{23} produced by IMF ionizing spectra which assume that the temperatures of the stars are (1) a function $T(M, Z)$ of both mass and metallicity and (2) a function $T(M)$ of mass only. The latter systematically overestimates the strength of the oxygen lines.

3. RESULTS

Figure 7 shows the average electron temperature as a function of metallicity. At very low abundances there are few coolants and the gas is hot. Collisionally induced Lyα dominates the cooling, though geometry plays a role in how efficient this mechanism is relative to other processes, such as free-free and free-bound radiation. At log (O/H) ≈ -3.9 ($\approx 0.15\ Z_\odot$), Lyα dominates diffuse geometries (low ϵ), while [O III] $\lambda\lambda$4949, 5007 is the most important coolant for high ϵ. As Z increases, oxygen dominates completely. The intensity of the optical forbidden lines reaches a maximum around log (O/H) ≈ -3.6 ($\approx 0.3\ Z_\odot$). As the number of coolants continues to increase, the temperature declines and the cooling burden shifts to the more readily excited infrared "fine-structure" lines. For $Z > Z_\odot$, the 52μ and 88μ lines of oxygen provide the plurality of the cooling, though many species contribute to the thermal balance.

As a result of this shifting of the cooling burden, R_{23} is sensitive to the metallicity. Since R_{23} forms a one-parameter sequence in oxygen abundance for $Z > 0.5\ Z_\odot$, the other nebular parameters $\bar{U}$ (geometry) and T (ionizing spectrum shape) must remain fixed with small scatter. However, a naïve implementation of this scheme fails in the sense that the models overestimate the strength of the oxygen lines for $Z > 0.5\ Z_\odot$. This is the result of using a fixed stellar temperature T at all Z. If one properly accounts for the effects of metallicity on the ionizing spectrum, R_{23} "turns over" more rapidly, as required by the data. This is demonstrated in Figure 8, which shows the locus of R_{23} for models ionized by clusters whose spectra were calculated with the $T(M, Z)$ relation discussed in § 2.1, and also for models where T is taken to be a function of mass only. (Until the appearance of Maeder's 1990 models, this was an obligatory assumption.) Note that M_u is not well defined in this case, as what is fixed is T_u, the hottest star in the cluster. Clearly, M_u must increase steadily with Z to maintain the same T_u. This is the reason for the failure of the naïve model, as recognized by Pagel et al. (1979) and MRS; the latters' attempt to parameterize the $T(Z)$ relation lacked the necessary information.

The locus of R_{23} for the entire model grid is shown in Figure 9. Individual model points have been connected with a cubic spline interpolation. There are three distinct regions in this diagram, which we will refer to as the "upper branch" for log (O/H) > -3.4 ($Z > 0.5\ Z_\odot$), the "turnover region" for $-3.9 <$ log (O/H) < -3.4, and the "lower branch" for log (O/H) < -3.9 ($Z < 0.15\ Z_\odot$). Along the upper branch, where R_{23} was originally identified as an abundance indicator, the intensity of the optical oxygen lines steadily declines with increasing metallicity. All the models converge towards the same upper branch line, R_{23} being relatively insensitive to $\bar{U}$ and T in this region of the diagram. This is simply a result of the declining importance of λ3727 and $\lambda\lambda$4959, 5007 to the thermal balance of the nebulae. In the turnover region, R_{23} is sensitive to $\bar{U}$ and, to a lesser extent, to T, but is insensitive to Z. Here, λ3727 and $\lambda\lambda$4959, 5007 dominate the physics of the nebulae and hence are sensitive to the details of the geometry and ionizing spectra. Along the lower branch, R_{23} is sensitive to both Z and $\bar{U}$, but T is relatively unimportant for spectra produced by a cluster IMF, in contrast to models which use a single stellar spectrum to define T. This is because a spectrum

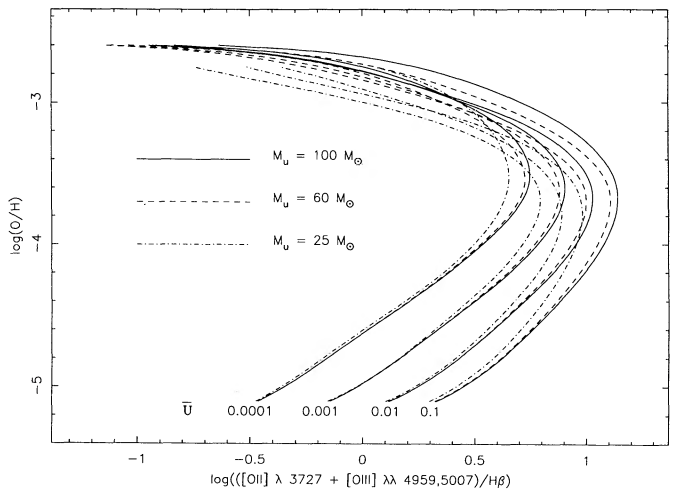

FIG. 9.—Calibration of R_{23} as an abundance indicator. Lines are as per Fig. 6; different $\bar{U}$ are labeled.

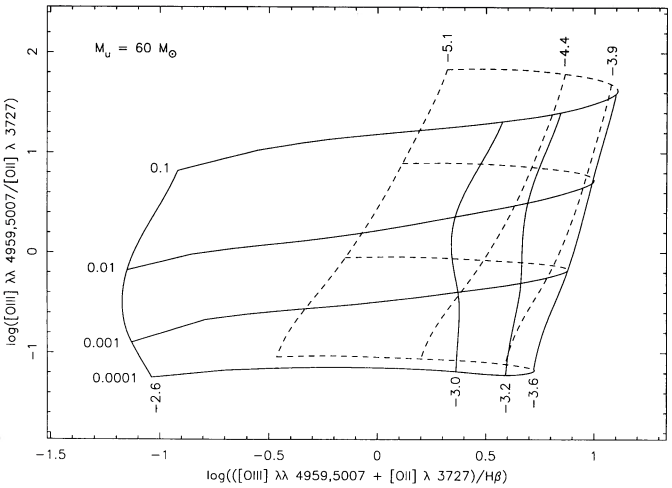

FIG. 10.—Model grid plotted in the observable [O III]/[O II] vs. R_{23} plane. These line ratios are particularly effective at separating the nebular parameters $\bar{U}$ and Z. Numeric labels refer to lines of constant $\bar{U}$ (horizontal) and constant log (O/H) (vertical). Solid lines are the upper branch, dashed lines are the lower. Plotting [O III]/[N II] as a third dimension would resolve the ambiguity between the branches and make this a single-valued two-dimensional surface embedded in three dimensions. For clarity, only models with $M_u = 60\ M_\odot$ are plotted; similar, closely nested surfaces exist for other values of this parameter.

produced by an IMF has appropriate contributions from the entire mass range, and so changes in M_u have less effect than when only one T is represented.

Except in the turnover region, R_{23} is a good abundance indicator. Along the upper branch, R_{23} converges on the same value for all $\bar{U}$ and M_u. On the lower branch, $\bar{U}$ is important and R_{23} must be supplemented with additional information. This is available in the strong oxygen lines. The ratio of [O III] $\lambda\lambda$4949, 5007 to [O II] λ3727 is much more sensitive to $\bar{U}$ than to M_u or Z. Figure 10 shows the power of [O III]/[O II] when combined with R_{23} to separate the effects of $\bar{U}$ and Z. Thus the strong oxygen lines contain the necessary information for determination of accurate abundances on the lower branch.

Of course, the fact that that there is an upper and lower branch means that R_{23} is double valued. The abundance indicator [O III]/[N II] proposed by Alloin et al. (1979) is useful for determining which branch is appropriate. Though the calibration of this indicator is uncertain because it depends on the nucleosynthetic origin of nitrogen and the details of the local star-formation history, it is monotonic and varies by over one order of magnitude between the upper and lower branches. Hence this additional piece of information is sufficient for determining which branch is appropriate for a particular object.

4. DISCUSSION

The calibration of R_{23} presented here is compared to previous calibrations in Figure 11. Our upper branch calibration is similar to previous ones (which are based on models at high metallicity), with the scatter expected due to differences in $\bar{U}$ and T explicitly included. In the turnover region, agreement is much worse. This is due to selection effects in the data used for the various calibrations and to the fact that R_{23} no longer forms a simple one-parameter sequence for $Z < 0.5\ Z_\odot$. The calibration of EP is too low due to the lack of calibration data with $Z > 0.5\ Z_\odot$. That of MRS is too high for the same reason. The two differ only in how the authors chose to connect the data available at low Z to the models at high Z. The calibration of TPF is based on very few points from one galaxy (M101). These are the most recent of many abundance estimates for M101 (see Shields & Searle 1978; Rayo, Peimbert, & Torres-Peimbert 1982; MRS; Evans 1986), and are rather low because they have corrected their data for the nonlinearity of the IIDS. While this procedure may be appropriate for this detector, the temperature indicating line ratios, and hence the derived abundances, are very sensitive to it. On the lower branch, the EP calibration roughly parallels the theoretical track for typical high-ionization ($\bar{U} = 0.01$) nebulae, which is remarkable considering that their lower branch calibration is based solely on I Zw 18. The lower branch calibration of S89 is somewhat too flat. This is due to his restriction to data of $Z < 0.1\ Z_\odot$, necessary to guarantee being on the lower branch. Most of the data is near the upper limit, and a change in this restriction would have a powerful influence on the derived slope. His inability to find a dependence of R_{23} on $\bar{U}$ is due to the dearth of data and nearly orthogonal effects of $\bar{U}$ and Z in this part of the diagram.

There is reasonable agreement between our calibration and that of DE. However, their calibration is based on a very different physical mechanism. They hypothesize the existence of a correlation between $\bar{U}$ and Z, for which they fit a relation to the data. This supposed correlation is based on the behavior of the [S II] λ6731 line, which is difficult to model (see discussion in S89). Also, an apparent $\bar{U}$-Z correlation can be caused by observational selection effects (see below). Furthermore, there is no compelling physical reason to believe such a correlation exists. The possibilities they discuss are (1) a metallicity dependent IMF, (2) dust, and (3) environmental effects. We have shown that the behavior of the oxygen lines can be modeled with an appropriate $T(Z, M)$ relation without the need to invoke a varying IMF. That DE found no variation in stellar temperature with metallicity is due to the decreasing sensitivity of the nebular spectrum to $T > 40{,}000$ K and the limited set of data on which this conclusion was based (Evans & Dopita 1985, see their Figs. 11–14). Dust has the opposite effect of what is required (see § 2.4), as they realized. The last possibility is most plausible, supposing that the filling factor depends on metallicity as the result of radiation pressures on metal lines, or

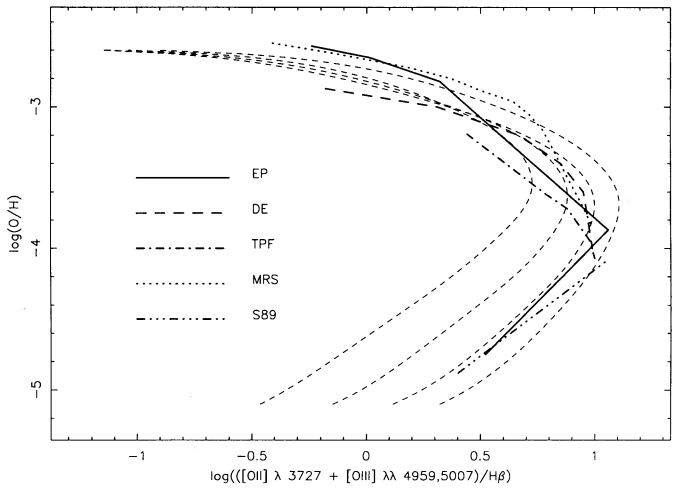

FIG. 11.—Comparison of previous calibrations of R_{23} to that presented here. For clarity, only models with $M_u = 60\ M_\odot$ are plotted here. Other lines are as per Fig. 1.

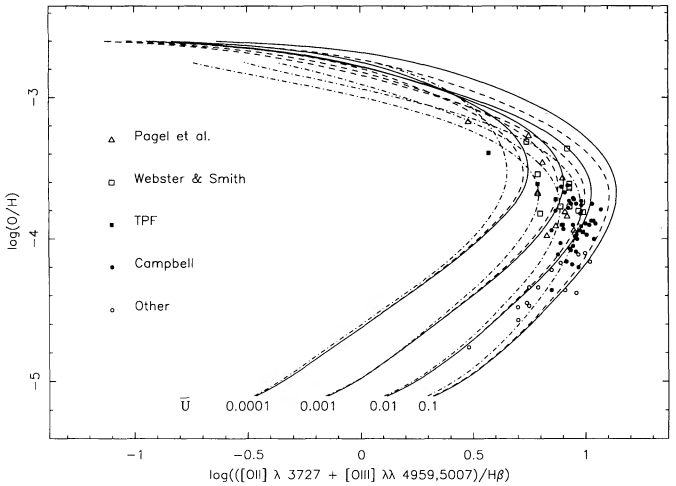

FIG. 12.—Comparison of our R_{23} calibration with data. Lines are as per Fig. 6; different $\bar{U}$ are labeled. The symbols refer to data listed in Table 2. That the data appear to turn over more rapidly than the models is a selection effect (see text).

that the gas density is systematically higher in high-metallicity regions. However, Lyα is the dominant source of radiation pressure in our models at all Z, so the former is at most a minor effect, while the latter depends on galaxy type. In contrast, our models are governed by a $T(Z, M)$ relation *expected* from stellar physics, and produce reasonable results *independent* of the data. Even if a $\bar{U}$-Z correlation exists, it would not alter our calibration since the effects of various $\bar{U}$ are explicitly included.

Data from the literature are plotted against our calibration in Figure 12. For a fair comparison, the oxygen abundance must be determined by means other than the strong line "empirical" method which we are trying to calibrate. Therefore, we limit the comparison data set to objects whose abundances have been determined with a temperature-sensitive line ratio, usually [O III] $\lambda\lambda$4959, 5007/λ4363. The data and their sources are listed in Table 2. This very heterogeneous data set is subject to a number of severe selection effects and analysis differences which will be discussed in detail below. Typical errors are 0.1–0.2 dex in log (O/H), except for the data of Campbell (1988), for which the errors are less than 0.05 dex. Figure 12 reveals that the data provide virtually no constraint on the calibration of R_{23}.

Most of the data are in the turnover region. This confinement encourages the unphysical sharp turn around of the Edmunds & Pagel (1984) calibration. However, it is a natural selection effect resulting from λ4363 being most easily measured when the oxygen lines are strong. That the lower half of the turnover region is more fully populated than the upper half is a similar selection effect. That is, λ4363 must be measured for

TABLE 2

DATA

Object	O/H	[O II]/Hb	[O III]/Hb	R_{23}	ref.	Object	O/H	[O II]/Hb	[O III]/Hb	R_{23}	ref.
NGC 1365 #4	-3.17	0.37	-0.12	0.48	1	POX 108	-3.90	-0.06	0.98	1.02	6
NGC 300 #1	-3.27	0.56	0.29	0.75	1	Tol 1345-420	-3.90	0.22	0.86	0.95	6
NGC 300 #7	-3.31	0.35	0.51	0.74	2	Tol 0645-376	-3.90	0.29	0.77	0.90	6
NGC 55 #3	-3.36	0.72	0.49	0.92	2	Tol 2	-3.90	0.35	0.76	0.90	6
M 101 S3	-3.39	0.41	0.07	0.57	3	POX 139	-3.91	0.17	0.91	0.98	6
NGC 7793 W11	-3.46	0.50	0.52	0.81	4	NGC 6822 HuX	-3.91	0.20	0.76	0.87	5
NGC 300 #11	-3.54	0.53	0.46	0.79	2	POX 4 NW	-3.93	0.40	0.74	0.90	6
NGC 1313 #5	-3.57	0.22	0.80	0.90	5	UM 469	-3.94	0.04	0.92	0.98	6
M 101 S7	-3.61	0.33	0.61	0.79	3	Fairall 30	-3.94	0.25	0.73	0.85	6
NGC 55 #2	-3.61	0.42	0.77	0.93	2	NGC 6822 Ho15	-3.94	0.30	0.84	0.95	5
NGC 5253 B	-3.62	0.57	0.67	0.92	6	M 101 S13	-3.95	0.12	0.92	0.99	3
Tol 1116-325	-3.63	0.14	0.81	0.89	6	POX 4	-3.97	-0.08	0.97	1.01	6
NGC 55 #1	-3.63	0.23	0.84	0.93	2	Tol 1304-386	-3.97	0.01	0.91	0.96	6
NGC 55 #7	-3.64	0.42	0.77	0.93	2	UM 462	-3.98	0.16	0.88	0.95	6
Tol 1004-296NW	-3.67	0.17	0.82	0.91	6	NGC 7793 W13	-3.98	0.65	0.35	0.83	4
NGC 300 #4	-3.67	0.71	0.01	0.79	1	Tol 0513-393	-4.00	-0.19	1.01	1.04	6
NGC 7793 DV132	-3.68	0.32	0.60	0.79	4	Camb 1148-203	-4.00	-0.08	0.92	0.96	6
POX 36	-3.71	0.43	0.79	0.95	6	Camb 0840+120	-4.03	0.16	0.80	0.89	6
Tol 1457-262 B	-3.72	0.17	0.87	0.95	6	POX 105	-4.05	0.10	0.88	0.95	6
M 101 S10	-3.72	0.49	0.64	0.87	3	Camb 0357-392	-4.07	-0.09	0.89	0.93	6
UM 483	-3.73	0.33	0.88	0.98	6	I Zw 36	-4.08	-0.15	0.90	0.94	6
Tol 0440-381	-3.73	0.38	0.78	0.93	6	POX 120	-4.09	-0.10	0.92	0.96	6
Camb 1409+120	-3.75	0.15	0.97	1.03	6	NGC 2363	-4.10	-0.24	0.97	1.00	7
Tol 1324-276	-3.75	0.18	0.88	0.96	6	Mrk 36	-4.11	-0.11	0.83	0.88	6
Tol 1457-262 A	-3.75	0.31	0.82	0.94	6	DDO 47	-4.11	0.00	0.92	0.97	8
NGC 5253 A	-3.76	0.16	0.91	0.98	6	Camb 1543+091	-4.16	-0.24	0.89	0.92	6
NGC 5253 #1	-3.77	0.30	0.77	0.89	2	Mrk 600	-4.16	0.22	0.94	1.02	9
NGC 300 #15	-3.77	0.46	0.75	0.93	2	DDO 64	-4.17	0.14	0.81	0.89	9
Fairall 2	-3.78	0.30	0.81	0.92	6	POX 186	-4.18	-0.39	0.92	0.94	6
Tol 1008-286	-3.79	0.05	1.03	1.07	6	Tol 1304-353	-4.20	-0.44	0.95	0.97	6
NGC 5253 #4	-3.80	0.17	0.89	0.97	2	WLM	-4.22	0.23	0.73	0.85	10
Tol 1004-296SE	-3.80	0.35	0.71	0.87	6	HI 1225+01	-4.34	0.13	0.64	0.75	11
NGC 5253 #3	-3.81	0.09	0.93	0.99	2	DDO 167	-4.34	0.31	0.61	0.79	8
NGC 6822 HuV	-3.81	0.19	0.82	0.91	5	Tol 1214-277	-4.36	-0.65	0.84	0.85	6
Tol 0633-415	-3.82	0.24	0.89	0.98	6	A1228+12	-4.36	0.11	0.84	0.91	9
NGC 300 #5	-3.82	0.60	0.38	0.80	2	A2228-00	-4.38	-0.08	0.92	0.96	9
NGC 1313 #7	-3.84	0.56	0.67	0.92	5	A1116+51	-4.45	0.31	0.54	0.74	9
II Zw 40	-3.87	-0.08	0.99	1.03	6	Tol 1223-359	-4.47	-0.01	0.67	0.75	12
Tol 1334-326	-3.87	0.05	0.99	1.04	6	Sextans A	-4.48	0.29	0.48	0.70	8
UM 439	-3.89	-0.12	1.02	1.05	6	Gr 8	-4.57	0.37	0.43	0.70	13
Tol 1924-426	-3.89	0.18	0.93	1.00	6	I Zw 18	-4.76	-0.48	0.43	0.48	14

NOTE.—All entries are logarithmic.

REFERENCES.—(1) Pagel et al. 1979; (2) Webster & Smith 1983; (3) TPF; (4) EP; (5) Pagel et al. 1980; (6) Campbell 1988; (7) Peimbert, Peña, & Torres-Peimbert 1986; (8) Skillman, Kennicutt, & Hodge 1989; (9) Kinman & Davidson 1981; (10) Skillman, Terlevich, & Melnick 1989; (11) Salzer et al. 1991; (12) Kunth & Sargent 1983; (13) Skillman et al. 1988; (14) Davidson & Kinman 1985.

a point to be plotted. Since there is a significant difference in electron temperature ($\approx$ 3000 K, see Fig. 7) across the turnover region, it is much more likely that λ4363 will be detected in the hotter, lower abundance objects, which are the only ones to be plotted. Hence the appearance that the data turn over at lower abundance than the models is due to this selection effect.

Other effects play a role as well. Except for the data of Campbell (1988), the oxygen abundances have been determined by standard methods (Osterbrock 1989). Campbell has determined the oxygen abundances for the objects in her sample by finding a best-fit model, and finds that this gives an abundance typically 0.2 dex larger than indicated by standard methods. This is reflected in Figure 13, which plots the abundance determinations from our R_{23} calibration against the published values. Good agreement is obtained with the data of Campbell (1988), while our determination of log (O/H) is typically 0.2 dex higher than those values obtained with a temperature sensitive line and the assumption of isothermality. We attribute this discrepancy to the failure of the isothermal assumption. This is because the production of λ4363 is biased towards high-temperature regions, leading to an overestimate of the average electron temperature and an underestimate of the abundance. Two-zone models suffer this same failing, though to a lesser extent. A better approach might be to assume some typical value for the temperature fluctuation parameter t^2 (Peimbert 1967). The standard method assumes that this is zero, but finite values of t^2 always increase the derived abundance. Since the models naturally include the temperature structure of the nebulae, they return systematically higher abundances.

Another reason for the failure of the isothermal assumption may be the presence of shocks in the ionized gas. Peimbert, Sarmiento, & Fierro (1991) have investigated the effects of shocks from supernovae and stellar winds on H II region spectra. They find that substantial enhancements in λ4363 can result for plausible shock strengths, while the strong lines (λ3737 and $\lambda\lambda$4959, 5007) are virtually unaffected. This will also have the effect of causing the standard method to underestimate the oxygen abundance.

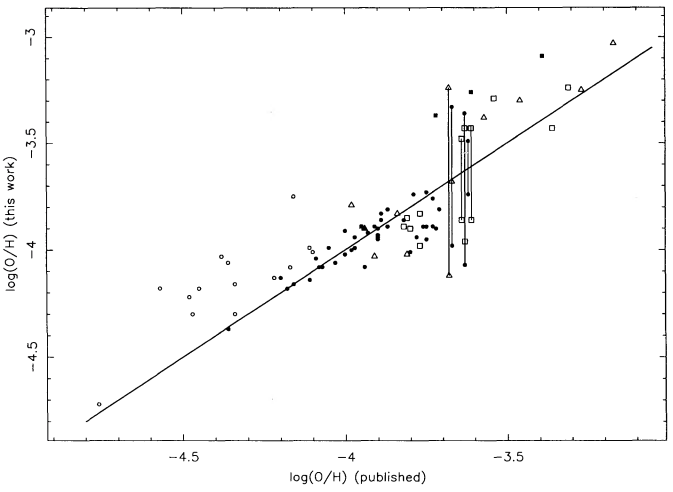

FIG. 13.—Comparison of oxygen abundances determined with our R_{23} calibration with published values based on temperature-sensitive line ratios. Points connected by vertical lines are double-valued because of the ambiguity of R_{23} in the turnover region. That some data fall above the line of equality results from assumptions made in the analysis by the original authors (see text). Symbols are as per Fig. 12.

The accuracy of our R_{23} calibration can be estimated by consideration of the uncertainties in the inputs. Relevant sources of error include the uncertainty in the stellar population, in $T(Z, M)$, in the stellar atmospheres, in the IMF, and in the nonhomologous effects of density at low excitation. Other possible sources of error are the adopted elemental abundances ratios, the atomic data employed, and the presence of shocks and dust. These latter are insignificant compared to the former, unless they represent an unsuspected systemic effect, such as gross errors in the atomic data. In the following we estimate the magnitude of the dominant errors.

Along the upper branch, the uncertainty in the stellar radiation field dominates. This is affected by both M_u and the choice of stellar atmospheres. From Figure 9, the spread in log (O/H) from a central choice of M_u is around 0.05 dex. The spread induced by the choice of stellar atmospheres can be estimated from the models of Evans (1991), which show the effects of different model atmospheres. Typically, these differences result in R_{23} values which correspond to 0.05 dex in log (O/H), the worst case being 0.08 dex (at the lowest $\bar{U}$ and T). Another important source of uncertainty is in the nonhomologous effects of density. Oey & Kennicutt (1991) estimate that R_{23} varies by amounts corresponding to 0.05 dex in log (O/H) for densities which vary a reasonable range from the value assumed here. The errors resulting from the uncertainties in $T(Z, M)$ and in the stellar population are harder to estimate, but are probably smaller than the 0.03 dex which we adopt here. Combining these in quadrature, and making a nominal allowance for the other sources of error, we estimate that the accuracy of the upper branch calibration is 0.10 dex. This would be worse if these effects systematically conspired to push the abundance determination in the same direction. While the choice of atmospheres seems to cause the abundance to be slightly overestimated because their radiation field is too hard (Evans 1991), the other uncertainties appear to have no preferred direction. Indeed, one can use other information present in the nebular spectrum to estimate M_u, greatly reducing its contribution to the uncertainty.

Since the choice of stellar atmospheres has a systematic effect, a brief digression is warranted. The effect occurs because the NLTE atmospheres of Mihalas (1972) lack real metal edges. These would introduce an additional source of spectral softening with increasing metallicity which might affect the exact position of the upper branch. However, this is a minor effect compared to the $T(Z, M)$ relation, and cannot cause a sharper turnover in R_{23} as the turnover region covers too small a range in Z for the edges to change much, and the values of M_u were chosen so that a substantial softening occurs in the turnover region anyway (recall Fig. 5). While R_{23} is only weakly affected by the metal edges, the relative amount contributed to it by [O II] and [O III] is sensitive to them, especially to the O^+ ionization edge near 2.6 Ryd. This makes the value of $\bar{U}$ determined from [O III]/[O II] uncertain, but only at high metallicity where $\bar{U}$ is unimportant to the determination of Z. Clearly, a set of OB star model atmospheres which is more comprehensive than any currently available in the literature is required for further progress on this topic.

On the lower branch, no error source is larger than 0.03 dex in log (O/H). While $\bar{U}$ is important in this region, the uncertainty in model [O III]/[O II] ratios in this region is low as the O^+ edge is weak at low Z (see Fig. 10 of Evans 1991). Adding

all sources of error in quadrature gives an uncertainty estimate of 0.05 dex. There is sufficient data in Figure 13 to check this. Restricting the comparison to Campbell's (1988) data on the lower branch [log (O/H) ≤ -3.9; a total of 23 objects], we find that the rms of the residuals between her abundances and ours is 0.05 dex with no zero-point offset, confirming the accuracy of our calibration.

In the turnover region the situation is worse, as expected from the compression of lines of constant Z in Figure 10. For all data in the turnover region, the rms is 0.2 dex. Most of this uncertainty is contributed by data within 0.1 dex of the apex [log (O/H) = -3.6], where considerable ambiguity can occur as to which side of the apex a particular object belongs (points connected with lines in Fig. 13). This ambiguity can only be resolved with an accurate measurement of T_e, or independent knowledge of the other nebular parameters.

While our grid is meant to model giant H II regions which are ionized by large clusters, application to the Orion nebula yields log (O/H) = -3.14 ± 0.10, which is essentially the solar abundance. This is consistent with the determination of Peimbert & Torres-Peimbert (1977). They measure the temperature fluctuation parameter t^2, and discuss its effect on the derived oxygen abundance. For $t^2 = 0$, log (O/H) = -3.48, which is roughly half solar. For $t^2 = 0.035$ (their preferred value), log (O/H) = -3.25, which is higher but still below solar. For the Peimbert & Costero (1969) value, $t^2 = 0.055$, log (O/H) = -3.08, which is slightly above solar. From simple considerations of galactic chemical evolution, a subsolar abundance for Orion is difficult to accept since it is a young object in the solar neighborhood where most of the stars are of solar metallicity. Given the uncertainty in t^2, we consider our value of the oxygen abundance in Orion to be a success. Since temperature fluctuations always increase the derived abundance, and spatially resolved temperature information is never available in extragalactic work, we believe that oxygen abundances can be derived from our calibration of R_{23} with reliability at least comparable to that obtainable with the direct method.

Even with accurate abundances, it is important to consider all applicable selection effects when interpreting the data. For example, the data of Campbell (1988) are selected from objective prism surveys by the strength of the [O III] $\lambda\lambda$4959, 5007 lines. This corresponds roughly to a vertical line in Figure 14, which is included for comparison to her Figure 1. Contrary to Campbell's claim, the lack of points with strong [O III] in the upper part of the turnover region (0.3–0.5 $Z_\odot$) is a selection effect. While the entire sample referred to by Campbell, Terlevich, & Melnick (1986) is selected by the presence of strong [O III], the subset of that sample for which abundance determinations have been made is selected by the presence of [O III] λ4363 (a horizontal line in Fig. 14). The fact that nebulae of higher abundance have lower electron temperatures prevents the detection of λ4363 and hence excludes them from Figure 14, even if they have strong [O III] $\lambda\lambda$4959, 5007 emission. This results in the restriction of Campbell's (1988) data to log (O/H) < -3.6, where the dominant source of cooling depends strongly on geometry. For diffuse, low $\bar{U}$ objects, collisionally induced Lyα dominates. As $\bar{U}$ increases, the cooling shifts to [O III] $\lambda\lambda$4959, 5007. This leads to a selection effect which favors high $\bar{U}$ objects at low Z, which is exactly what is seen in her data. Similar selection effects also occur in the data set employed by DE. Thus there is no convincing evidence of a $\bar{U}$-Z correlation which is not attributable to observational selection effects.

Note that the cluster ionizing spectra calculated using the

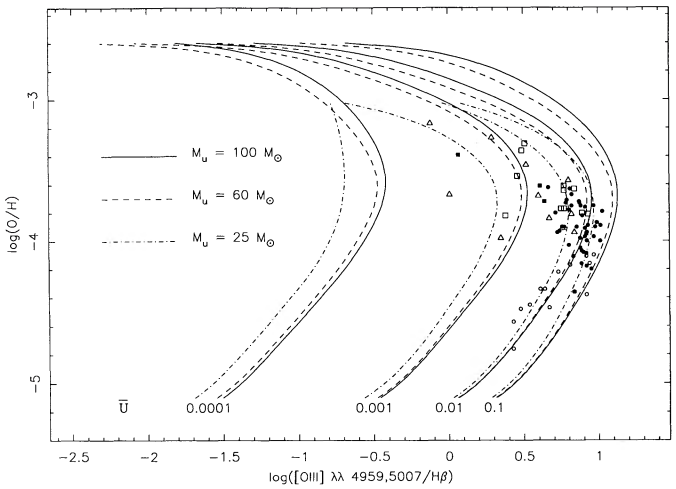

FIG. 14.—Comparison of model [O III]/Hβ to data. Note that the trend of stellar temperature increasing with decreasing metallicity implied by Campbell's (1988) Fig. 1 is naturally accounted for by the $T(Z, M)$ relation employed here. Also note the sensitivity of this line ratio to $\bar{U}$. Lines are as per Fig. 6; different $\bar{U}$ are labeled. Symbols are as per Fig. 12.

$T(Z, M)$ relation naturally account for the presence of hotter stars at lower metallicities implied by Campbell's (1988) Figure 1. Since the stars are automatically hotter at lower metallicity, there is no need to invoke a top-heavy IMF to explain this result. Likewise, there is no reason to suppose that M_u declines as Z increases (Shields & Tinsley 1976), or that Γ is in any way a function of Z. Finally, Figure 14 demonstrates that [O III]/Hβ alone is not a good metallicity indicator, though it is often used as such in the literature.

5. CONCLUSIONS

We have constructed an extensive, homogeneous grid of giant H II region models. We find that the abundance-sensitive line ratio $R_{23} \equiv$ ([O II] λ3727 + [O III] $\lambda\lambda$4959, 5007)/Hβ is a good metallicity indicator at high Z, and also at low Z when combined with the ratio of [O III] $\lambda\lambda$4959, 5007/[O II] λ3727. Physically, the reason R_{23} succeeds as an abundance indicator is the stellar mass-temperature-metallicity relation $T(Z, M)$. There is no need to invoke a metallicity-dependent IMF. Using the $T(Z, M)$ relation of Maeder (1990), we provide a calibration of R_{23} which is comparable in accuracy to that obtainable by direct methods.

This calibration should be particularly useful for determining abundances in large samples with rapidly obtainable low S/N data. For more precise work on individual objects, our model grid is useful for an initial estimate of O/H and $\bar{U}$. With the volume of parameter space restricted by this determination, it becomes practical to construct models with various stellar spectra and elemental abundances until an optimal fit is obtained.

Future work will include application of these methods to H II regions in low surface brightness galaxies. These span a range of surface density and gas mass fraction not exhibited by normal galaxies, thus providing a unique window on galaxy chemical evolution. We will also extend our model grid as improved input information becomes available (especially stellar atmospheres), and investigate the behavior of other lines. These include prominent ultraviolet and infrared emission lines available from satellite (*HST*, SIRTF) data, and the strong [S III] lines in the near-infrared. There is hope that this

latter, in the form of the η parameter of Vilchez & Pagel (1988), will allow unambiguous separation of the nebular parameters M_u, $\bar{U}$ and Z when combined with [O III]/[O II] and R_{23}.

We thank Gary Ferland for making his photoionization code generally available. Dave Silva provided endless encouragement in the pursuit of this project, and invaluable assistance in putting the CLOUDY output in a tenable form. The powerful plotting package of Diab Jerius greatly simplified the task of putting this information in graphical form. It is a pleasure to acknowledge helpful discussions with many others: Robert Kennicutt, Joel Bregman, Greg Bothun, Jim Schombert, John Salzer, Ted von Hippel, Chris Mihos, and Salley Oey.

REFERENCES

Abia, C. & Rebolo, R. 1989, ApJ, 347, 186
Alloin, D., Collin-Souffrin, S., Joly, M., & Vigroux, L. 1979, A&A, 78, 200
Campbell, A. 1988, ApJ, 335, 644
Campbell, A., Terlevich, R., & Melnick, J. 1986, MNRAS, 223, 811
Davidson, K., & Kinman, T. D. 1985, ApJS, 58, 321
Dopita, M. A., & Evans, I. N. 1986, ApJ, 307, 431 (DE)
Dufour, R. J., Garnett, D. R., & Shields, G. A. 1988, ApJ, 332, 752
Edmunds, M. G., & Pagel, B. E. J. 1984, MNRAS, 211, 507 (EP)
Evans, I. N. 1986, ApJ, 309, 544
———. 1991, ApJS, in press
Evans, I. N., & Dopita, M. A. 1985, ApJS, 58, 125
Ferland, G., & Truran, J. W. 1981, ApJ, 244, 1022
Kennicutt, R. C. 1983, ApJ, 272, 54
Kennicutt, R. C., Edgar, B. K., & Hodge, P. W. 1989, ApJ, 337, 761
Kinman, T. D., & Davidson, K. 1981, ApJ, 243, 127
Kunth, D., & Sargent, W. L. W. 1983, ApJ, 273, 81
Maeder, A. 1990, A&AS, 84, 139
Martin, P. G., & Ferland, G. J. 1980, ApJ, 235, L125
Massey, P., Parker, J. W., & Garmany, C. D. 1989, AJ, 98, 1305
McCall, L. M., Rybski, P. M., & Shields, G. A. 1985, ApJS, 57, 1 (MRS)
Mihalas, D. 1972, Non–LTE Model Atmospheres for B and O Stars (Boulder: National Center for Atmospheric Research), NCAR-TN/STR-76
Oey, M. S., & Kennicutt, R. C. 1991, in preparation
Osterbrock, D. E. 1989, Astrophysics of Gaseous Nebulae and Active Galactic Nuclei (Mill Valley: University Science Books)
Pagel, B. E. J., & Edmunds, M. G. 1981, ARA&A, 19, 77
Pagel, B. E. J., Edmunds, M. G., Blackwell, D. E., Chun, M. S., & Smith, G. 1979, MNRAS, 193, 219
Pagel, B. E. J., Edmunds, M. G., & Smith, G. 1980, MNRAS, 193, 219
Pagel, B. E. J., Terlevich, R., & Melnick, J. 1986, PASP, 98, 1005
Peimbert, M. 1967, ApJ, 150, 825
Peimbert, M., & Costero, R. 1969, Bol. Obs. Tonantzintla y Tacubaya, 6, 29
Peimbert, M., Peña, M., & Torres-Peimbert, S. 1986, A&A, 158, 266
Peimbert, M., Sarmiento, A., & Fierro, J. 1991, PASP, in press
Peimbert, M., & Torres-Peimbert, S. 1977, MNRAS, 179, 217
Rayo, J. F., Peimbert, M., & Torres-Peimbert, S. 1982, ApJ, 255, 1
Salzer, J. J., Alighieri, S. D. S., Matteucci, F., Giovanelli, R., & Haynes, M. P. 1991, AJ, in press
Searle, L. 1971, ApJ, 168, 327
Shields, G. A., & Searle, L. 1978, ApJ, 222, 821
Shields, G. A., & Tinsley, B. M. 1976, ApJ, 203, 66
Skillman, E. D. 1989, ApJ, 347, 883 (S89)
Skillman, E. D., Kennicutt, R. C., & Hodge, P. W. 1989, ApJ, 347, 875
Skillman, E. D., Melnick, J., Terlevich, R., & Moles, M. 1988, A&A, 196, 31
Skillman, E. D., Terlevich,R., & Melnick, J. 1989, MNRAS, 240, 563
Stasinska, G. 1990, A&AS, 83, 501
Talbot, R. J., & Arnett, W. D. 1974, ApJ, 190, 605
Tomkin, J., Sneden, C., & Lambert, D. L. 1986, ApJ, 302, 415
Torres-Peimbert, S., Peimbert, M., & Fierro, J. 1989, ApJ, 345, 186 (TPF)
Vilchez, J. M., & Pagel, B. E. J. 1988, MNRAS, 231, 257
von Hippel, T., & Bothun, G. 1990, AJ, 100, 403
Webster, B. L., & Smith, M. G. 1983, MNRAS, 204, 743